Molecular Therapy
Methods & Clinical Development
Original Article

Peptide-encoding gene transfer to modulate intracellular protein-protein interactions

Toshihiko Taya,[1] Daisuke Kami,[2] Fumiya Teruyama,[2,3] Satoaki Matoba,[1] and Satoshi Gojo[2]

[1]Department of Cardiovascular Medicine, Graduate School of Medicine, Kyoto Prefectural University of Medicine, Kyoto, Japan; [2]Department of Regenerative Medicine, Graduate School of Medicine, Kyoto Prefectural University of Medicine, Kyoto, Japan; [3]Pharmacology Research Department, Tokyo New Drug Research Laboratories, Kowa Company, Ltd, Tokyo, Japan

Peptide drug discovery has great potential, but the cell membrane is a major obstacle when the target is an intracellular protein-protein interaction (PPI). It is difficult to target PPIs with small molecules; indeed, there are no intervention tools that can target any intracellular PPI. In this study, we developed a platform that enables the introduction of peptides into cells via mRNA-based gene delivery. Peptide-length nucleic acids do not enable stable ribosome binding and exhibit little to no translation into protein. In this study, a construct was created in which the sequence encoding dihydrofolate reductase (DHFR) was placed in front of the sequence encoding the target peptide, together with a translation skipping sequence, as a sequence that meets the requirements of promoting ribosome binding and rapid decay of the translated protein. This enabled efficient translation from the mRNA encoding the target protein while preventing unnecessary protein residues. Using this construct, we showed that it can inhibit Drp1/Fis1 binding, one of the intracellular PPIs, which governs mitochondrial fission, an important aspect of mitochondrial dynamics. In addition, it was shown to inhibit pathological hyperfission, normalize mitochondrial dynamics and metabolism, and inhibit apoptosis of the mitochondrial pathway.

INTRODUCTION

How to target intracellular protein-protein interactions

Various intracellular protein-protein interactions (PPIs) are involved in essential biological processes, so they could be targets for intervention in the treatment of pathological alterations. According to interactome analysis, there are as many as 650,000 intracellular PPIs.[1] Currently, direct intervention in intracellular PPIs is very challenging,[2] while the development of drugs to extracellular PPIs, such as receptors on cell membranes and the ligand, has yielded significant results.[3] PPIs are characterized by a relatively flat binding surface over a large area. Low-molecular-weight compounds that have been developed as therapeutic drugs target extremely small regions, such as the active center of an enzyme reaction, which can be compared with a key and keyhole.[4] In contrast, antibody drugs intervene in biological processes by recognizing the exposed portions of proteins with high specificity.[5] Although a number of monoclonal antibody drugs have reached clinical use, there are significant barriers to their introduction into cells.[6] Peptide therapeutics, with insulin as the first example, have been applied in the clinic drugs that are few in number but high in importance. The development of PPI modulators or inhibitors is being intensively investigated as a strategy for further drug discovery.[7] In particular, for those proteins that have been identified as hot spots in the regions of interaction between two proteins, peptides possessing one of the amino acid sequences are expected to act as competitive inhibitors for the PPI, and various peptides have been shown to be effective in basic research.[8] Thus far, modifications have been developed based on sequence to improve stability, cell membrane permeability, and binding ability,[9] as have mimetics in which the backbone is replaced with artificial materials.[10] In addition, cyclic peptides, which are more cell permeable than linear peptides, show great potential.[11] Nevertheless, the cell membrane is still an extremely large barrier to modification of intracellular PPIs, and the cyclic form and modification of peptides pose problems specific to each peptide. Thus, a standardized methodology has not yet been generalized, and an alternative new platform methodology is needed to intervene in intracellular PPIs.

Genetic engineering

Although the introduction and production of proteins into human cells is commonly achieved through genetic engineering techniques, the intracellular expression of peptides that are less than 50 amino acids in length has been a challenging feat. Endogenous peptide hormones such as vasopressin secreted *in vivo* are most often translated as pre- or prohormones and then enzymatically truncated to peptides.[12] The most common industrial methods are chemical synthesis for short peptides and genetic engineering for longer proteins to be produced by cells. Previously, as an example of peptide drug discovery, recombinant DNA of glucagon-like peptide 1 (GLP-1), a short peptide of 30 amino acid residues, was introduced into yeast, and the secreted protein was purified from the supernatant, leading to drug discovery.[13] However, it has been reported that, in mammalian cells, ribosome binding to mRNAs with coding sequences less than 400 nucleotides in length decreases linearly, and binding becomes

Received 25 September 2023; accepted 24 February 2024;
https://doi.org/10.1016/j.omtm.2024.101226.

Correspondence: Satoshi Gojo, Department of Regenerative Medicine, Graduate School of Medicine, Kyoto Prefectural University of Medicine, 465 Kajii cho, Kamigyo ku, Kyoto 6028566, Japan.
E-mail: gojos@koto.kpu-m.ac.jp

worse as the coding sequence length becomes shorter, with almost no binding at 114 nucleotides.[14] Even in the case of GLP-1, some studies on gene therapy schemes have used vectors in which the coding sequence of GLP-1 alone is a transgene, but the expression efficiency is not high.[15,16] Research on gene therapy targeting angiotensin II or IV with even shorter lengths of 9 or 7 amino acid residues has used fusion proteins with Ig Fc portions.[17] In that study, a furin cleavage site was placed between the Ig Fc and the transgene angiotensin so that angiotensin II could be excised after secretion and function as a peptide. Similarly, a fusion protein construct with Ig Fc has been used in gene therapy for vasopressin.[18] Protease-based peptide excision for fusion proteins is based on the *in vivo* mechanism and is a reasonable choice when targeting secreted peptides.[19] However, when intracellular PPIs are targeted, there are major concerns about the side reactions of the remaining Ig Fc and other proteins.

Mitochondrial fission

To examine methods of intervention in intracellular PPI, mitochondrial fission was chosen as the target. Its dynamics have a great impact on mitochondrial quality control, and it could be a drug target.[20,21] In fission, which separates degraded mitochondrial fractions, an intracytoplasmic protein called Drp1 associates with several adaptor proteins, including Fis1, on the mitochondrial outer membrane to form a ring around the mitochondrion.[22] The ring is subsequently mechanically contracted by the action of GTPases, and Mfs is involved in completion of disassociation to complete fission. In various pathological processes, such as ischemia-reperfusion injury and neurodegenerative diseases, excessive fission has been reported to be involved in further exacerbating the pathology.[23] P110, 7-amino-acid peptide that represents a homologous sequence between Fis1 and Drp1(8), can suppress hyperfission, resulting in improvement of disease.[24] As with many other peptide preparations, P110 has not yet reached the clinical stage due to a major hurdle in the efficiency of its introduction into cells.

Working hypothesis

In this study, we developed a novel method to intervene in intracellular PPI by introducing nucleic acids encoding dihydrofolate reductase from *Escherichia coli* (ecDHFR), which was used as a ribosome binding fragment, rather than as a switch to regulate protein expression, and a gene of interest. After translating the transgenes, ecDHFR was rapidly degraded by the ubiquitin proteasome system (UPS), resulting in no adverse effects. Using this strategy, we attenuated the hyperfission of mitochondria, which led to suppression of apoptosis under conditions of doxorubicin-induced cardiotoxicity. The results of this study demonstrate that this novel recombinant construct provides a platform for targeting intracellular PPIs.

RESULTS

Validation of peptide expression via recombinant gene transfer

Since there are few antibodies for peptides, we decided to validate the peptide gene delivery system using split GFP (Figure 1A).[25] GFP is formed from 11 β strands and excites fluorescence, and a system has been developed to decompose GFP into 1–10 and 11 strands and excite fluorescence when two polypeptides combine to form a proper conformation. In the reported study, the 11th β strand was expressed in cells as a fusion protein, FLAG-14-3-3ζ-GFP11 (8, 244, and 16 amino acid residues, respectively). In this study, we created the following system to express the peptide of interest by itself instead of such a fusion protein. To express the peptide of interest, we decided to use ecDHFR, which has been frequently used to regulate spatiotemporal gene expression (Figure 1B). This protein is rapidly degraded by the UPS after translation. The destabilizing domain (DD) of DHFR, which is responsible for the decay, is stabilized by trimethoprim (TMP) to avoid digestion by the UPS. The TMP interacts with Ile(5), Asp(27), Ser(49), Ile(94), Tyr(100), and Thr(112) of ecDHFR.[26] DHFR has been widely used as an on switch in basic research. In this study, the DHFR coding sequence played a role as a ribosome-binding fragment instead of a switch (Figure 1C). A construct was created by connecting the sequence that causes ribosome skipping, P2A, downstream of DHFR and placing the sequence that encodes the peptide to be expressed downstream of P2A as a single unit (this unit is hereinafter referred to as the peptide expression unit [PEU]) (Figure 1C). The PEU produced two separate translation products, DHFR and the peptide of interest, but the translated DHFR decays quickly due to the DD of DHFR, so it is assumed that only the peptide of interest will be expressed in the cell into which PEU is introduced.

Cells expressing GFP β strands 1–10 were generated using HeLa cells as hosts, and fluorescence microscopy confirmed that GFP emission was not observed and that GFP1-10 mRNA was expressed (Figure 1D). We transfected the cells with a plasmid expressing only GFP11 using mCherry-carrying plasmid as a control for gene transfer (Figure S2A). In contrast, when gene transfer was performed with an expression plasmid incorporating PEU (CD-G11 PEU), which contains a fusion protein with mCherry placed upstream of DHFR as a marker for gene transfer, mCherry expression occurred in the presence of TMP. Most of the mCherry-positive cells were found to be GFP positive (Figure 1E). Since this assay was performed using plasmid vectors, which have limited gene transfer efficiency, the mCherry-DHFR fusion protein was used to analyze only the cells in which gene transfer took place and was examined in the presence of TMP. The gene-transferred cells were examined by FACS. Similar to the fluorescence microscopy results, GFP was expressed only at low intensity in a very small number of cells with the GFP11-only expression vector, whereas with PEU most mCherry-expressing cells were GFP positive, and the fluorescence intensity was approximately three times higher than that of GFP11 alone (Figures 1F and 1G). Next, mRNA expression in these gene-transferred cells was examined by RT-qPCR. GFP1-10 mRNA expression in the host cells was constant, and GFP11 mRNA expression was significantly higher in the GFP11 alone expression vector than in the group transfected with the expression vector with PEU (Figure 1H). These results indicated that the transcription efficiency of the vectors was better with the shorter expression unit GFP11, but when the coding sequence was short, such as for a peptide, it did not lead to polypeptide abundance. The PEUs constructed in this study enabled cells to express polypeptides with short chain lengths at high efficiency by gene transfer.

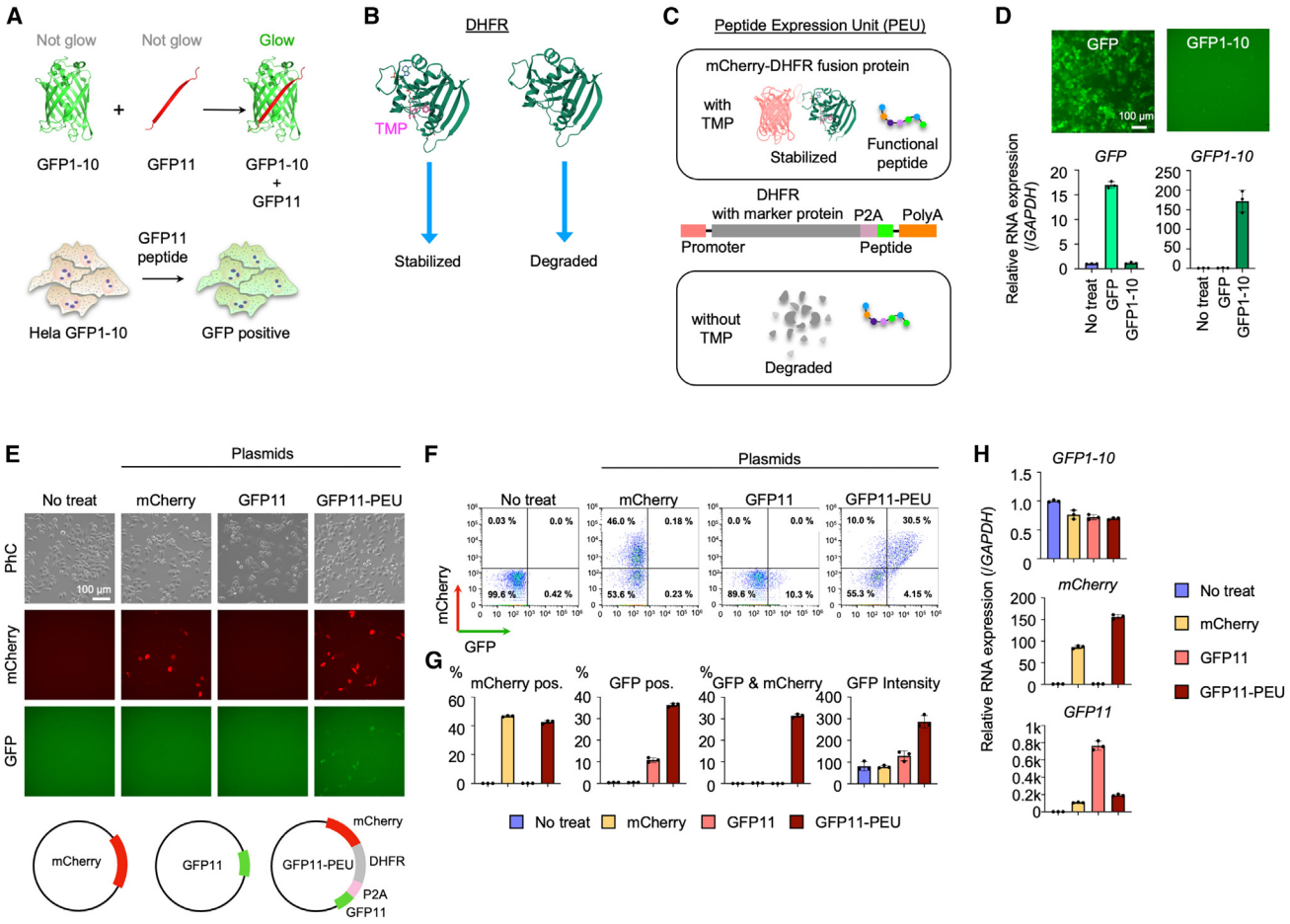

Figure 1. Demonstration of peptide expression of the developed PEU

(A) Split GFP model was constructed to confirm the presence of the introduced peptide in the cells. GFP1–10 or GFP11 do not fluoresce on their own, but do if they coexist and form an appropriate conformation. HeLa cells that constantly express GFP1–10 were generated. (B) A model of the DHFR peptide. TMP can stabilize the DHFR peptide and DHFR fusion protein. (C) Structure of the PEU, showing that in the absence of TMP, which stabilizes DHFR, DHFR or fusion proteins with DHFR decay rapidly, while peptides that underwent ribosomal skipping at P2A remain. (D) No fluorescence was observed in HeLa cells expressing GFP1–10, but the mRNA of GFP1–10 was confirmed. (E–G) Gene transfer of PEU with GFP11 and a sequence encoding a fusion protein of mCherry and DHFR (GFP11 PEU) showed GFP fluorescence in GFP1–10-expressing cells, indicating that GFP11 was translated. Plasmid transfection of GFP11 did not show fluorescence (E). FACS analysis showed that a lot of mCherry-positive cells were GFP positive with high fluorescence intensity, indicating that P2A connects translation downstream to express the peptide (F and G). (H) GFP11 PEU had lower mRNA expression levels compared to gene transfer of the plasmid coding GFP11.

DHFR degradation

We verified that DHFR, which is necessary for maintaining the ribosome binding required for peptide translation, is rapidly disrupted after translation. In the absence of TMPs, little mCherry and little GFP were observed, with weak expression intensity (Figure 2A). In contrast, the addition of TMPs revealed mCherry-positive cells, many of which showed a high intensity of GFP. This observation was also obtained by FACS (Figures 2B and 2C). This confirmed that proteins translated from Dhfr mRNA for ribosome binding stabilization rapidly decayed in the absence of TMPs, as expected.

To confirm the nature of P2A, genes encoding two fluorescent proteins were connected across P2A and G7, and fluorescence was used to measure their expression levels. The expression plasmids were introduced into the cells (Figure S1B). The correlation ratio of mCherry and GFP was produced and it was not statistically ruled out that G7 and P2A are equivalent (Figures 2D and 2E).

mRNA encoding P110 suppressed LPS-induced hyperfission

When considering the clinical application of PEU, we decided to verify whether it could be used as an mRNA medicine. To perform this verification, we selected P110 to confirm the phenotypic transformation induced by targeted peptide expression. Mitochondrial dynamics have been reported to provide the basis for a variety of diseases.[27] Among them, the regulation of hyperfission is deeply

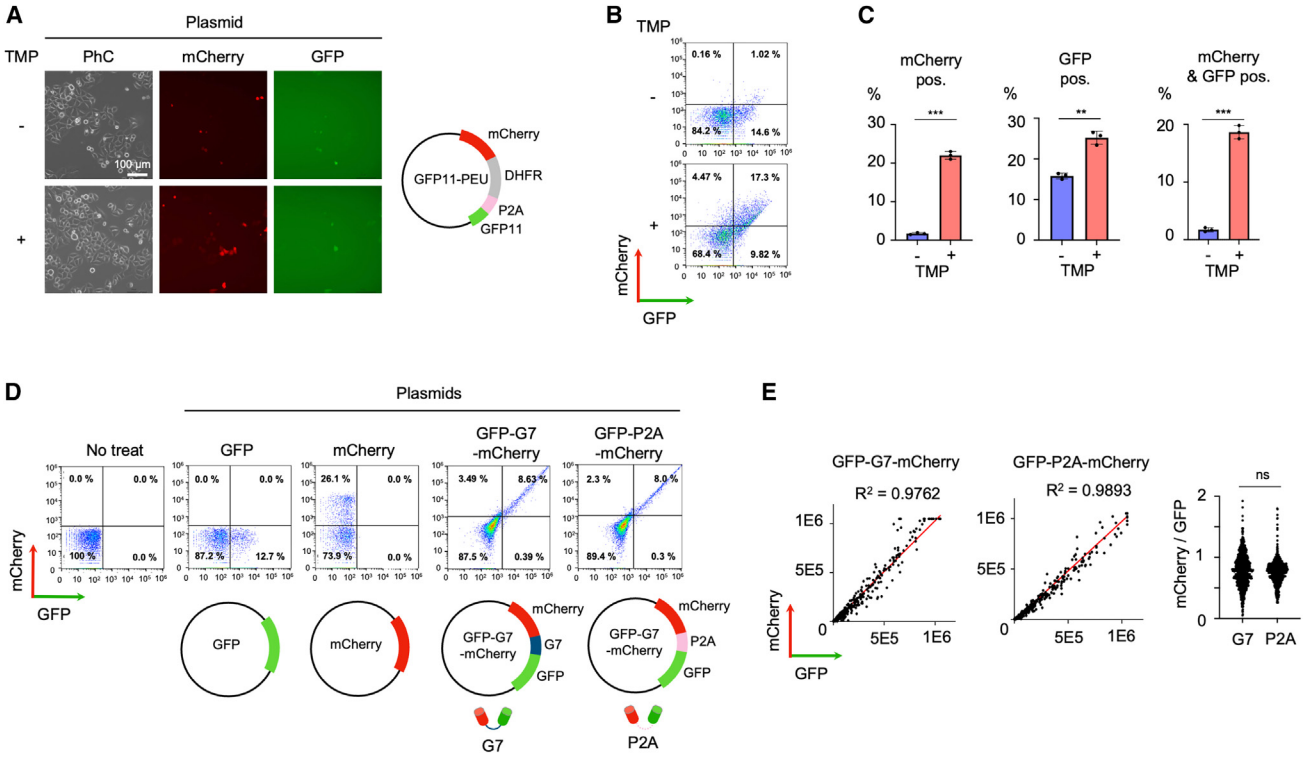

Figure 2. Functional analysis of DHFR and P2A used for PEU

(A–C) GFP11 PEU plasmid was transfected into GFP1–10-expressing HeLa cells, and mCherry and GFP forming a fusion protein with DHFR were observed with or without TMP, a stabilizer for DHFR, by fluorescent microscopy. Without the addition of TMP, mCherry fluorescence was attenuated, but GFP fluorescence was confirmed, indicating that P2A separates upstream and downstream translation (A). Fluorescence was quantified by FACS. In the absence of TMP, mCherry was almost quenched, but GFP fluorescence remained, consistent with fluorescence microscopy results (B and C). (D and E) To confirm the function of P2A, fluorescence was observed using a construct in which P2A was replaced with the G7 sequence as a control, and the correlation between the two fluorescence signals was not significantly different between P2A and G7, indicating that P2A induces ribosomal skipping but does not significantly affect downstream translation. **p < 0.01, ***p < 0.001. ns, not significant.

involved in cell death associated with external environmental stresses such as infections and mitochondrial dysfunction; as a regulatory protein of fission, DRP1 plays a role in mitochondrial disconnection by polymerizing and associating with FIS1(24). P110 was developed as a peptide that could suppress hyperfission and thus cell death by inhibiting this association.[8] However, the major barrier to its introduction into cells has hindered its clinical application. This is a problem faced by many therapeutic peptides. In this study, CD-G11 PEU was transfected into H9c2 cardiomyoblasts via a lipofection method (Figure S1B). The sequence of P110 was determined by codon optimization and replaced GFP11 of CD-G11 PEU with P110 (CD-P110 PEU). As the external stressor causing hyperfission, lipopolysaccharide (LPS) was chosen (Figure S1B). We chose mitochondrial dynamics to show that PEU, a peptide-encoding sequence separated by DHFR and P2A, can intervene in intracellular PPI. The pathological state of hyperfission induced by Drp1 and Fis1 PPIs can be inhibited by a seven amino acid residue peptide, P110(8). We transfected cells with PEU mRNA carrying P110 and observed phenotypic changes *in vitro*. The cardiomyoblast cell line H9c2 was selected because P110 suppresses hyperfission in cardiac reperfusion injury,[23] and LPS was used to induce mitochondrial fission *in vitro*.[28] H9c2 with constant expression of GFP1-10 was created, and PEU mRNA with mCherry-GFP11 was gene transfected. The mCherry-positive transgenic cells were GFP positive in both microscopy (Figure 3A) and FACS (Figures 3B and 3C), confirming that GFP11 was effectively translated. Exposure of H9c2 cells to LPS was confirmed to significantly alter mitochondrial dynamics (Figure 3D). The transfected P110 PEU mRNA has mCherry as a fusion protein with DHFR as a gene transfer marker. mCherry was stabilized by adding TMP to distinguish PEU-transfected cells from non-transfected cells for functional evaluation. LPS induced mitochondrial fission, and quantification of mitochondrial morphology showed that the branch length was short and that the number of branches was high. The mitochondrial morphology was normalized by transfection of H9c2 with PEU containing mCherry-P110 (Figure 3E). LPS exposure increased mitochondrial reactive oxygen species, but gene transfer of P110 abolished this increase (Figure 3F). In contrast, intervention with P110 increased the mitochondrial membrane potential per unit volume (Figure 3F). This is thought to be an inhibitory effect on mitophagy, which also suppresses the hyperactivity of mitophagy.

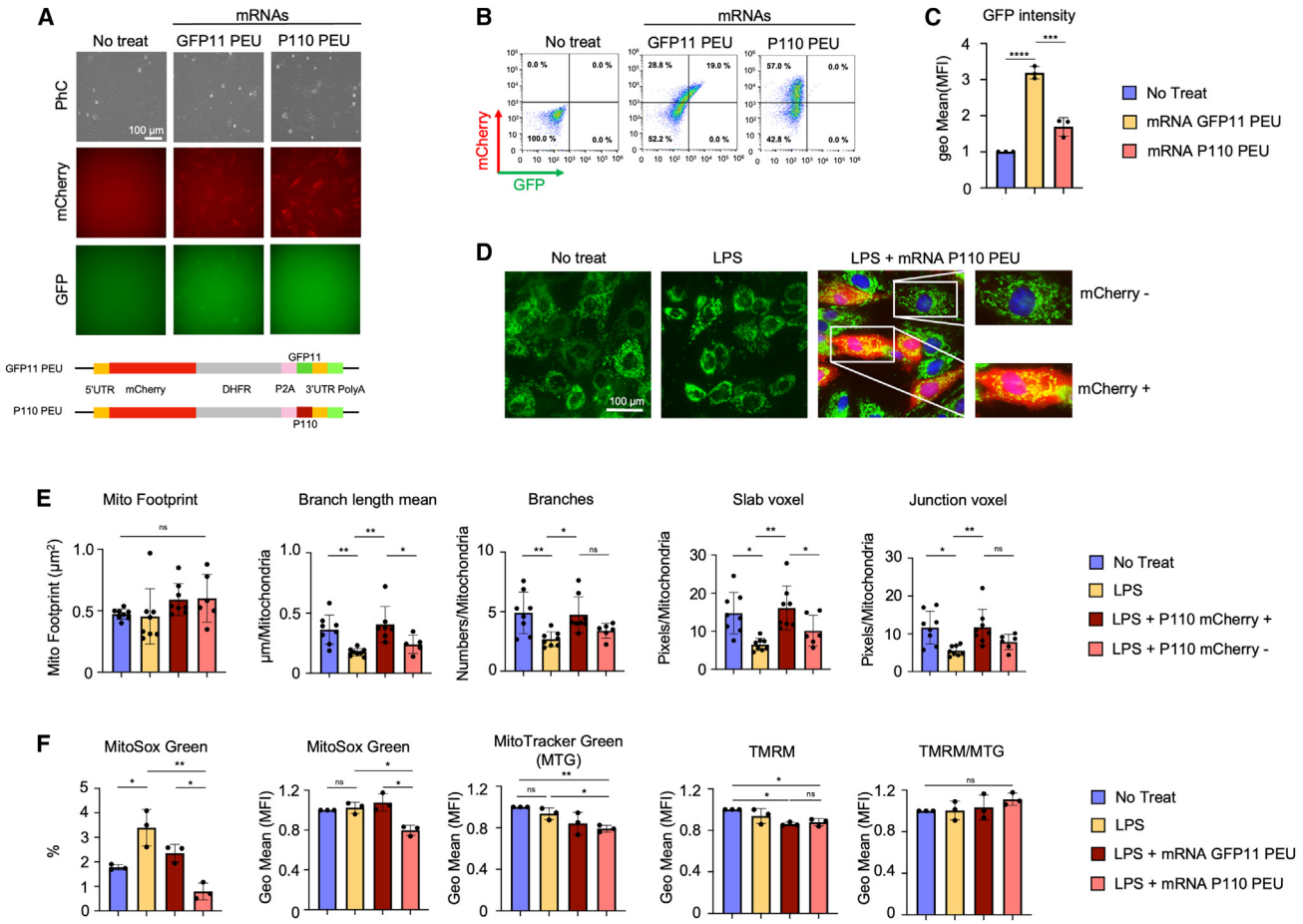

Figure 3. Improvement of mitochondrial dysfunction by gene transfer of P110 PEU mRNA

(A–C) Cardiomyoblast H9c2 cells, which constitutively express GFP1–10, were generated and gene transfected with P110 or GFP11 PEU mRNA. These constructs have mCherry as a fusion protein of DHFR as a gene transfer marker. mCherry-positive cells in which gene transfer took place were GFP positive in GFP11 PEU mRNA group. No GFP fluorescence was observed in P110 PEU mRNA group (A). In FACS, the results of fluorescence microscopy were similarly accepted (B), and fluorescence intensity was quantified, confirming that GFP fluorescence intensity was significantly stronger in GFP11 PEU mRNA (C), and peptide expression in PEU mRNA was validated. (D and E) Effect of P110 PEU mRNA on mitochondrial dysfunction by addition of LPS in H9c2. Compared with cells transfected with PEU mRNA (mCherry-positive cells) and not transfected (mCherry-negative cells), mitochondrial morphology by Mito tracker green staining showed that the network was preserved in the former and fragmentation was more pronounced in the latter (D). Mitochondrial dynamics were quantified using MiNA. Mitochondrial volume (Mito footprint) did not change significantly in either group, but mean branch length, number of branches, area occupied by two branches (slab pixels), and area occupied by three branches (junctional pixels) were significantly decreased by LPS ($p = 0.0056$, 0.0047, 0.0052, and 0.0056, respectively), and significantly elevated by P110 PEU mRNA introduction compared with the LPS group ($p = 0.0016$, 0.0087, 0.0012, and 0.005, respectively) (E). Mitochondrial reactive oxygen species (ROS) measured with MitoSox was increased with LPS, and the introduction of P110 PEU significantly suppressed both the percentage of mitochondrial ROS positivity and its mean fluorescence intensity compared to the addition of LPS ($p = 0.0007$ and 0.0158, respectively). Mitochondrial membrane potential, corrected for mitochondria volume measured by Mitotracker Green, was not significantly altered by the P110 PEU intervention (F). *$p < 0.05$, **$p < 0.01$. ns, not significant.

mRNA encoding P110 suppressed doxorubicin-induced cell death

In this study, a model of doxorubicin exposure to H9c2 was selected as a system in which cell death is induced by mitochondrial hyperfission in response to external stress, and P110 was introduced as mRNA to examine whether it has a mitigating effect on cell death (Figure S1C). Doxorubicin is a typical drug that causes myocardial damage and can lead to doxorubicin cardiomyopathy, a treatment-resistant disease in clinical practice.[29] As with LPS exposure, mitochondrial staining was performed with MitoTracker Green, and morphology was quantified using mitochondrial network analysis (MiNA) (Figures 4A and S2).[30] Exposure to doxorubicin decreased footprints indicative of mitochondrial capacity; both the length and number of branches were significantly reduced, and the numbers of bifurcations and trifurcations were also significantly reduced (Figure 4B). In contrast, in the group transfected with P110 mRNA, all parameters were significantly increased compared with those in the doxorubicin group (Figure 4B). Next, we examined whether P110

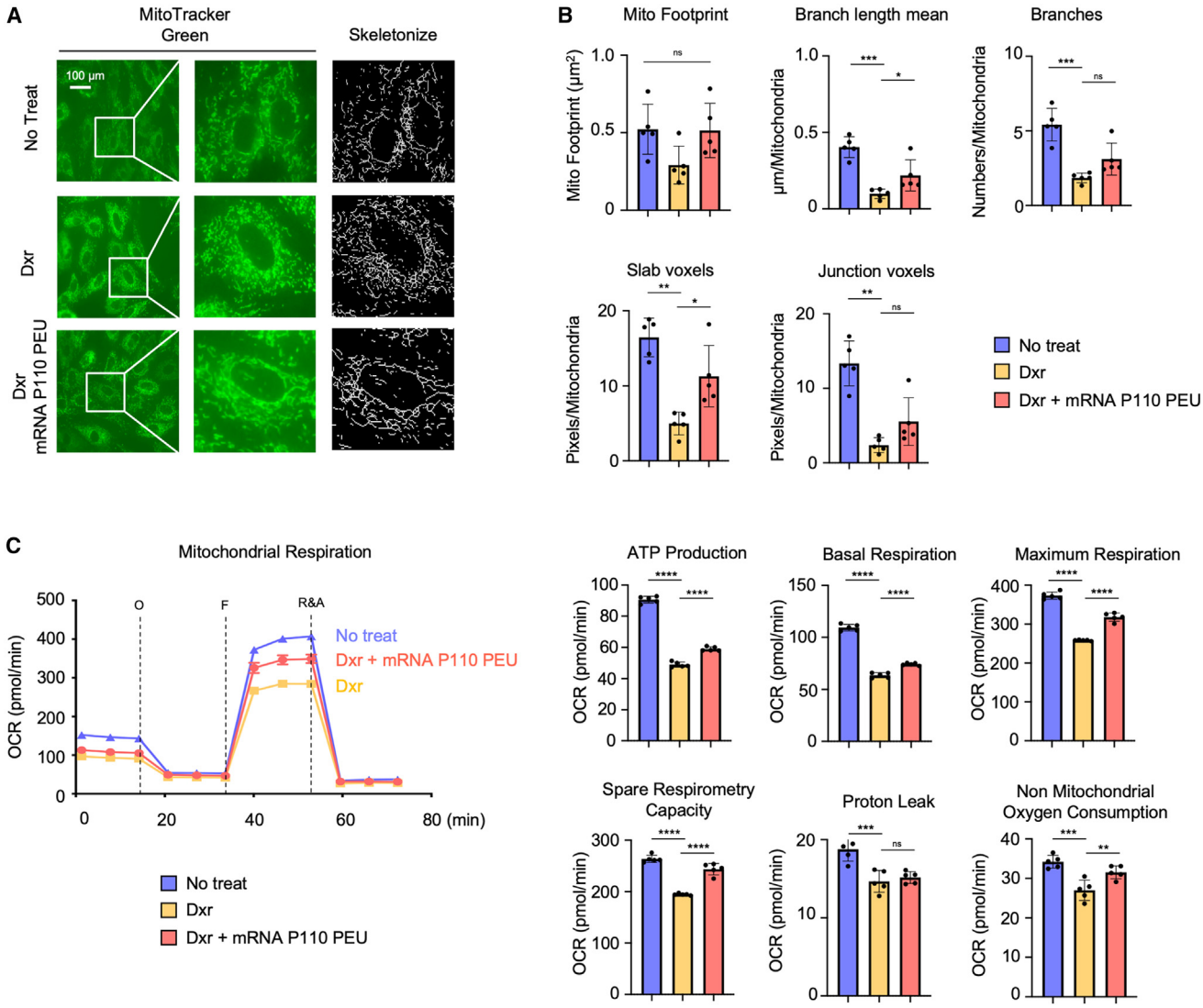

Figure 4. Doxorubicin (Dxr)-treated H9c2 cells were rescued from cell death with P110 PEU mRNA

(A and B) Mitochondrial fragmentation increased by Dxr and was suppressed by the introduction of P110 PEU, as observed by staining mitochondria with Mito tracker green and fluorescence microscopy (A). Dxr significantly decreased branch length ($p = 0.0001$), number of branches ($p = 0.0001$), and area occupied by two and three branches ($p = 0.0001$ for both slab and junctional pixels), indicating mitochondrial fragmentation. The introduction of P110 PEU significantly increased branch length ($p = 0.0356$) and area occupied by three branches ($p = 0.0119$) from the Dxr group. (C) The oxygen consumption rate (OCR) was measured using respiratory chain inhibitors (O, oligomycin; F, FCCP; R, rotenone; A, actinomycin) for the effect of P110 PEU mRNA on mitochondrial respiratory function. By Dxr addition, ATP production, basal respiration, maximum respiration, spare respiratory capacity, proton leak, and non-mitochondrial oxygen consumption were all significantly decreased ($p < 0.0001$). The introduction of the P110 PEU mRNA significantly increased all except for proton leak ($p < 0.0001$). *$p < 0.05$, **$p < 0.01$, ***$p < 0.001$; ****$p < 0.0001$. Ns, not significant.

suppression of hyperfission improved mitochondrial respiratory function. Doxorubicin exposure significantly decreased all parameters of basal respiration, maximum respiration, spare respiratory capacity, and ATP production. The P110 group showed a significant attenuation of the decrease and recovered to a level comparable with that in the control for spare respiratory capacity (Figure 4C). Proton leakage was decreased by doxorubicin exposure and slightly but significantly improved in the P110 group. Nonmitochondrial oxygen consumption also showed a similar trend, confirming that mitochondria function in concert with glycolysis (Figure 4C).

Cell death induced by doxorubicin exposure was assessed as double-positive staining upon co-staining with DAPI and annexin V. In the mock group with GFP11, there was evidence of impairment at gene transfer, while in the group with mRNA for P110, in addition to the cell death induction of doxorubicin, P110 also counteracted the

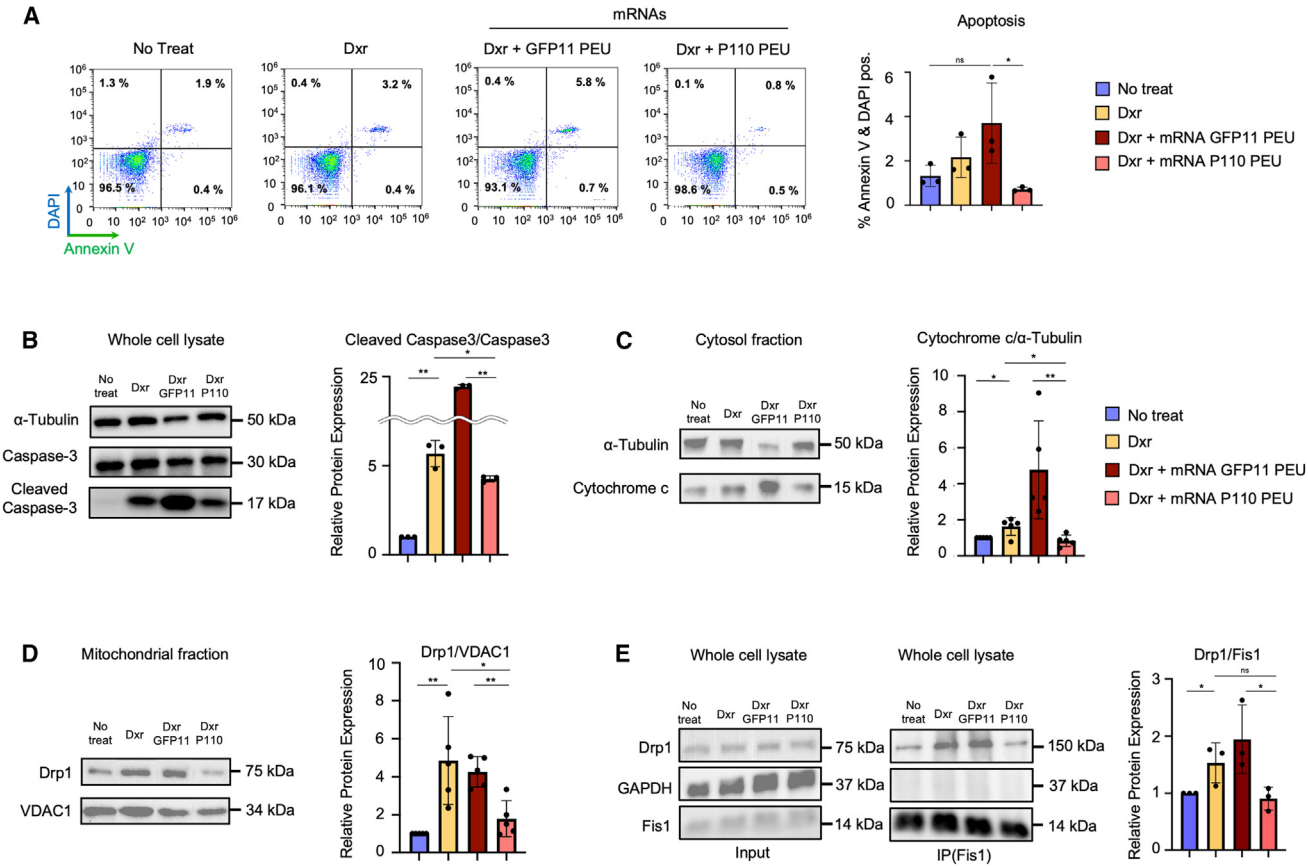

Figure 5. Inhibition of cell death by doxorubicin (Dxr) with P110 PEU mRNA and its mechanism of action

(A) Cell death upon Dxr exposure was assessed by double staining with annexin V and DAPI. Double-positive cells increased with Dxr exposure and decreased with Dox exposure plus P110 PEU mRNA. (B) Caspase-3 as an executor of cell death was evaluated by Western blotting. Cleaved caspase-3/caspase-3 ratio was significantly increased by Dxr exposure ($p < 0.0001$) and significantly decreased by introduction of P110 PEU mRNA ($p = 0.019$). (C) Cytochrome *c* of the mitochondria pathway in cell death was evaluated by western blotting. Cytochrome *c* was increased by Dxr exposure ($p = 0.01$) and decreased by the introduction of P110 PEU mRNA ($p = 0.0018$). (D) Mitochondrial fractions were used to quantify recruited Drp1 to mitochondria. Dxr exposure significantly increased Drp1 by ($p = 0.049$) and decreased by the introduction of P110 PEU mRNA. (E) Immunoprecipitation with Fis1, a counterpart of Drp1 in the mitochondrial outer membrane, was performed to quantify Drp1 associated with Fis1. In response to Dxr exposure, Drp1 was decreased by introduction of P110 PEU mRNA. *$p < 0.05$, **$p < 0.01$, ***$p < 0.001$. ns, not significant.

effect of cell death induction at gene transfer (Figures 5A and S3). We examined the activation of caspase 3, one of the final executors of cell death. Although our mRNA cell transfection method strongly induced cleaved caspase 3 expression over doxorubicin exposure, transfection with P110 reduced the impairment of both the gene transfer method and doxorubicin (Figures 5B and S4). Leakage of cytochrome *c* from mitochondria due to hyperfission triggered apoptosis and was one of the key factors in hyperfission-induced cell damage. The release of cytochrome *c* by mRNA gene transfer was not as potent as cleaved caspase 3 induction, but further enhanced doxorubicin-induced cytochrome *c* release, while transfection with P110 suppressed cytochrome *c* release (Figures 5C and S5). This indicated that the mitochondrial pathway was suppressed by P110, but that the extramitochondrial pathway for apoptosis was not well regulated by P110. The molecular mechanism of P110 is that it inhibits the recruitment of Drp1 to the mitochondrial membrane during fission. We quantified Drp1 in mitochondrial fractions to determine whether this mechanism was mediated by the introduction of P110 mRNA. The results showed that, while doxorubicin exposure caused Drp1 to accumulate very strongly in mitochondria, P110 treatment significantly prevented Drp1 aggregation, maintaining it at almost the same level as in the control group (Figures 5D and S6). To confirm that Fis1 is the assembly molecule for Drp1 accumulation at the mitochondrial membrane, immunoprecipitation with Fis1 followed by immunoblotting with Drp1 was performed as previously reported. Drp1 expression was significantly enhanced by doxorubicin exposure, and the situation remained the same in the mock group. In contrast, Drp1 was restored to almost control levels with little aggregation in the P110 induction group (Figures 5E, S7, and S8). In conclusion, P110 mRNA gene transfer inhibited the association of Drp1-Fis1, an intracellular PPI, preventing hyperfission that contributes to pathogenesis and reducing cell death.

DISCUSSION

In this study, we developed an expression unit that enables highly efficient intracellular production of peptides via a gene transfer scheme. Using this unit, a peptide named P110, which suppresses mitochondrial fission dynamics and consists of eight amino acid residues,[8] was produced in cells at a high rate. The fission inhibition shown when P110 was introduced into cells as a peptide[23,24] was reproduced upon both LPS stimulation and doxorubicin-induced cardiotoxicity, resulting in avoidance of cell death. This PEU has the potential to modulate any intracellular PPIs if an optimized nucleic acid sequence of the hot spot peptide mimics obtained from PPI protein structure analysis is inserted into the coding sequence site. It can be used a platform technology for drug discovery targeting intracellular PPIs. The PEU provides a new alternative strategy for peptide drug discovery, which has the major barrier of cell membrane permeation.

Peptide gene therapy

Peptides are a form of pharmaceuticals, most of which have their targets in the plasma membrane.[2,7] Although various efforts to deliver peptides into the cytosol that intervene in intracellular processes have been made to overcome their vulnerability and membrane impermeability *in vivo*,[31] a universal solution has not yet been found to give peptides the ability to pass through cell membranes and exist stably in the extracellular milieu, such as blood.[1,32] However, the use of viral vectors for gene transfer has become common, and various gene therapies have reached the clinical stage. Studies have been conducted to utilize gene transfer schemes to produce peptides intracellularly,[18] but most of them were designed as recombinant nucleic acids that are fusion proteins with IgG heavy chain constant region (IgG-Fc) portions to ensure stability as well as translation efficiency.[17,19] The basis of these studies seems to be that ribosome binding to nucleic acid sequences with coding sequence nucleotide lengths below 400 is significantly reduced, and only very limited binding can be achieved at lengths of approximately 100(14). In the reported peptide gene therapy technique, the target is a secreted peptide, and the strategy is to ensure translation efficiency with IgG-Fc and place a gene cleavage site between Fc Ig and the gene of interest. After secretion out of the cell, FcIg and the target peptide are split, and IgG-Fc is metabolized. Using this strategy to express the peptide intracellularly likely results in the accumulation of IgG-Fc inside the cell, potentially causing a stress response, which is inappropriate for intracellular targeting.

We hypothesized that, if the ribosome can stably bind to the mRNA and if the sequence that ensures subsequent translation is degraded after its role is complete, the nucleic acid can be used to efficiently express the peptide in a cell. One mechanism of protein decay in cells is degradation in the UPS. Two molecules have been reported among proteins with DDs targeted by UPS that are stabilized by binding of low-molecular-weight compounds: FK506/rapamycin-bidding protein, which is stabilized by a synthetic compound called Shld1,[33] and ecDHFR, which is stabilized by TMP.[34] These have been used for genome editing, stress response research, and regulation of protein expression *in vivo* and have provided a variety of insights. TMPs are widely used as antibiotics, are highly stable in the body, and have been shown to exhibit functions at low nanomolar levels. Until now, DDs have always been used as ON switches when TMP or a TMP analog is used.

One of the methods to produce two independent proteins from a fusion protein coding sequence is to insert a 2A peptide sequence,[35] in addition to a proteinase cleavage sequence between the two proteins.[36] This sequence was originally identified as a sequence that allows viruses to make multiple proteins from polycistronic sequences. Failure of the ribosome to make a peptide bond between proline and glycine results in the cleavage of the peptide chain. After peptide bond failure, the ribosome moves to the 3′ side to continue translation, which has been reported to be 20%–30% less efficient than translation on the 5′ side for protein-coding transgenes.[37] The 2A peptides have a single alphabet derived from the name of the identified virus. When P2A, which is derived from porcine teschovirus-1, was selected in this study, an 18-amino-acid residue derived from P2A was added to the C-terminal side of the polypeptide translated on the 5′ side, and a proline from P2A was added to the N-terminal side of the polypeptide translated on the 3′ side.

For peptides that function intracellularly, especially those that modify intracellular PPIs, there is one patent report of intracellular production by gene transfer using mRNA.[38] Via placement of multiple nucleic acid sequences encoding peptides in series, with the 2A sequence in between, the sequence length was increased in an attempt to improve translation efficiency. However, a report on the efficiency was not included, and whether the intervention caused a phenotypic transformation was not reported. In the present study, we examined three tandem GFP11 constructs with the P2A sequence in between and found that, although they were expressed, their protein expression levels were extremely low, and they did not seem to have the potential to induce phenotypic transformation.

PPIs

Interactome analysis has revealed as many as 650,000 intracellular PPIs.[1] Peptide drug discovery, despite significant technological developments such as peptidomimetics, is only beginning to approach the ability to target intracellular PPIs. Advances in structural analysis of PPIs have revealed that PPIs are formed by three motifs to be targeted: α-helices,[39] β-strands,[40] and turn regions. Many PPIs with α-helices occur between structured and unstructured proteins, and important proteins such as p53 take advantage of the plasticity of the unstructured regions to form a variety of robust structures.[41] Peptides that mimic these solid regions may have highly specific and effective inhibitory activity against such PPIs. One example is P110(8), the target of this study. Drug discovery using peptidomimetics methodology proposes multiple compounds for individual PPIs based on the structures and requires repeated screening to create a lead compound. Moreover, the process of optimization from a lead compound is time consuming.[42] Recent advances in substitution with unnatural amino acids[39]; the introduction of sidechain linkers,[9] which were reported to

be useful not only for stability but also for affinity enhancement[43]; and the development of macrocyclization[44] enable the further potentiation of peptide drugs. We previously found an association between DDX6 and 4ET, which plays a central role in RNA decay in RNA metabolism.[10] Subsequently, we found that RNA decay regulates adipogenic differentiation by inhibiting the intracellular PPI of DDX6 and 4ET using peptidomimetics with a novel cage-like chemical skeleton.[10] Peptides and peptidomimetics, including ours, can elicit useful effects against intracellular PPIs if they can be stably introduced into cells, but cell membrane permeation is a major barrier that limits peptide drugs from reaching the clinic. One example is ALRN-6924, which was developed to inhibit the association of the tumor suppressor p53 with its inhibitory proteins, MDM2 and MDMX. Thus far, ALRN-6924 has shown preclinical efficacy against leukemia,[45] phase I trials for solid tumors and lymphomas have been completed and reported, and a phase II trial is underway.[46] The fact that all peptide drugs approved by the U.S. Food and Drug Administration in the past decade have targeted receptors present in the cell membrane[47] speaks to the difficulty of peptide drug discovery for intracellular PPIs. In contrast, when nucleic acids are used in this platform, if the amino acid sequence of the binding region can be identified, it is possible to create the construct in a straightforward manner.[48] The fact that the construct design for an mRNA vaccine against severe acute respiratory syndrome coronavirus 2 (SARS-CoV-2) was completed within 3 weeks after the identification of the sequence of the spike protein indicates the superiority, usefulness, and feasibility of the methodology.[49,50]

RNA delivery

This study reported that P110 PEU mRNA functions *in vitro*. The future needs to demonstrate its usefulness in animal studies, but the problem is the RNA delivery system. RNA delivery has developed with various drug delivery systems, and better methods are still being developed.[51] RNA therapeutics can be divided into three main categories: small interfering RNA, antisense oligonucleotide, and mRNA, all of which have reached clinical application.[52] Therapy using mRNAs requires synthetic vehicles due to their long strand length. The SARS-CoV-2 vaccine using lipid nanoparticles has made a significant contribution to pandemic control worldwide.[49,50] Efficient delivery of mRNA to cells that constitute parenchymal organs other than skeletal muscle, such as the heart, kidney, and lungs,[53] and to the central nervous system[54] remains a major area of research. Recently, RNA delivery to hematopoietic stem cells by systemic delivery has been greatly improved by active targeting using antibodies against c-kit in combination with lipid nanoparticles, and it was reported that sickle cells could be treated.[55] Furthermore, *ex vivo* RNA transfer has also been demonstrated for RNA delivery to blood stem cells by lipid nanoparticles[56] and to T cells using polyelectrolyte core-shell nanoparticles.[57] Pathogenesis due to abnormal mitochondrial dynamics, the subject of this study, occurs in a variety of diseases,[58] and ischemia reflux injury (IRI) is a classic example of mitochondrial hyperfission leading to cell death.[23] However, the time course of IRI is extremely rapid, and current technologies present significant hurdles to efficiently delivering mRNA to target cells and inducing gene expression as the disorder progresses. If the established RNA delivery system is to be used, the liver may be the *in vivo* application of this study. Because mitochondrial hyperfission has been shown to play a major role in the pathogenesis of nonalcoholic fatty liver disease,[59] it may be appropriate to demonstrate P110 PEU. It has been reported that hematopoietic dysfunction in myelodysplastic syndromes is due to mitochondrial fragmentation.[60] P110 PEU mRNA transfection into hematopoietic stem cells may improve the pathogenesis of myelodysplastic syndrome.

Perspective

mRNA medicines have rapidly established themselves as middle-molecule drugs, and the targets of nucleic acid drugs other than those in gene therapy have expanded from the conventional regulatory mechanism of RNA metabolism to include proteins. In this study, we report a recombinant unit encoding a peptide that has not been targeted by nucleic acid drugs due to translation efficiency issues. Intracellular PPIs are involved in signaling cascades related to tumorigenesis within systems in which biological processes such as autophagy and the ubiquitin proteinase system are carried out by complexes of multiple proteins. In addition, the molecular basis of mRNA metabolism is regulated by liquid-liquid phase separation, which provides the molecular basis for the processing body and membraneless organelles such as stress granules and has a great impact on the formation of various pathological conditions. A platform that enables modification of intracellular PPIs using nucleic acids, which have been recognized as undruggable, will open the door to an extremely large field of drug discovery.

MATERIALS AND METHODS

Cell culture

HeLa and H9c2 were cultured in high-glucose DMEM (Fujifilm Wako Pure Chemical, Osaka, Japan) supplemented with 10% fetal bovine serum (Thermo Fisher Scientific, Waltham, MA, USA) and 1% penicillin/streptomycin (Thermo Fisher Scientific) and incubated at 37°C in a humidified 5% CO_2 incubator. The cells were seeded in growth medium in a Falcon 100-mm TC-treated cell culture dish (Corning, Corning, NY, USA).

Plasmid DNA construction

All plasmids were constructed using NEBuilder HiFi DNA assembly (New England Biolabs, Ipswich, MA, USA). We used pCAGGS, pcDNA3, and pMRNAxp, which were obtained from System Biosciences (Palo Alto, CA, USA), to generate either recombinant plasmids or mRNA. All plasmids were designed using Snap Gene software (Ver. 6.2, Dotmatics; Boston, MA, USA). The inserted fragments were GFP, mCherry, GFP11, P110, mCherry-P2A-GFP, mCherry-G7-EGFP, mCherry-ecDHFR-P2A-GFP11, and mCherry-ecDHFR-P2A-P110. These fragments were inserted into multiple cloning sites of the backbone vectors via NEBuilder Hifi DNA assembly. The ecDHFR sequence was designed and synthesized by Integrated DNA Technologies (Coralville, IA, USA). All sequence information is deposited in Zenodo: https://doi.org/10.5281/zenodo.10500256.

Fluorescence-activated cell sorting analysis

For flow cytometric analysis, cells were washed with PBS, harvested with 0.25% trypsin-EDTA and stained with DAPI (4′,6-diamidino-2-phenylindole, dihydrochloride, Dojindo Molecular Technologies, Kumamoto, Japan). The amount of fluorescent protein and dyes were detected using FACS at 405, 488, 561, and 638 nm lasers. For the apoptosis assay, we used the annexin V assay kit (Medical and Biological Laboratories Corporation, Tokyo, Japan) and DAPI solution. Fluorescence data were collected using an Attune Flow Cytometer (Thermo Fisher Scientific). The flow cytometry files were analyzed using FlowJo software (Ver. 10.8.2, Becton, Dickinson & Company, Ashland, OR).

mRNA synthesis

All mRNAs were constructed using an mMESSAGE mMACHINE T7 Transcription Kit (Thermo Fisher Scientific). Templates for mRNA synthesis were used on the sequence of the pMRNAxp mRNA Express vector plasmid with the gene of interest. Plasmid DNA was linearized with a restriction enzyme NdeI downstream of the polyA tail. Then, T7 2× NTP/ARCA, 10× T7 Reaction Buffer, T7 Enzyme Mix, and nuclease-free water were mixed thoroughly and incubated at 37°C for 2 h. One microliter of TURBO DNase was added and mixed well, and the reaction was incubated at 37°C for 15 min. Then, tailing reagents, which included E-PAP Buffer, 25 mM $MnCl_2$, ATP solution, and E-PAP, were added to the mixture, which was incubated at 37°C for 45 min. A Monarch RNA Cleanup Kit (New England Biolabs) was used to purify RNA from the mixed solution for *in vitro* transcription. A260/A280 is measured each time as a quality control for mRNA, and 2.0 or higher is used as a criterion for subsequent use of mRNA.

Gene transfection

One day before transfection, cells were seeded in six-well plates at 10,000 cells per well. For plasmid DNA transfection, 1 day after cell seeding, 50 ng plasmid DNA was mixed with diluted Lipofectamine 3000 Transfection Reagent (Thermo Fisher Scientific Incorporated) in Opti-MEM (Thermo Fisher Scientific) and incubated for 15 min at room temperature. Then, the solutions were added to the six-well plates and incubated for 2 days. For mRNA transfection, 1 day after cell seeding, 500 ng mRNA and Lipofectamine MessengerMAX Transfection Reagent in Opti-MEM (Thermo Fisher Scientific) were incubated for 5 min at room temperature. Then, the solutions were added to the six-well plates for 12 h.

Imaging of fluorescent proteins and dyes

One day before transfection, cells were seeded in a 35-mm glass base dish (IWAKI Corporation, Tokyo, Japan). One day after cell seeding, plasmid DNA and mRNA were transfected into the cells. After transfection, the EGFP- and mCherry-positive cells were visualized using BZ-X800 (Keyence Corporation, Osaka, Japan). For mitochondrial morphology analysis, MitoTracker-Green FM (Thermo Fisher Scientific) and Hoechst 33342 (Dojindo Molecular Technologies) were added to the medium, and the cells were incubated for 30 min at room temperature. The cells were then thoroughly washed twice with PBS. The cells were viewed using a BZ-X800 (Keyence Corporation).

RNA isolation, RT-PCR, and qPCR

Total RNA from cells and tissues was extracted using TRIzol (15596018, Thermo Fisher Scientific) and a Direct-zol RNA MiniPrep Kit (R2052, Zymo Research, Irvine, CA, USA) with DNase I, according to the manufacturer's instructions. To perform the qRT-PCR assay, 100 ng total RNA was reverse-transcribed using a PrimeScript RT Reagent Kit (RR036A, Takara Bio, Shiga, Japan) and a T100 thermal cycler (Bio-Rad Laboratories). qRT-PCR was performed using the Kapa SYBR Fast qPCR Kit Master Mix (2×) Universal (KK4602, Kapa Biosystems Ltd., Wilmington, MA, USA) on a CFX connect real-time system (Bio-Rad Laboratories, Hercules, CA, USA). Relative gene expression levels were normalized to human or rat *GAPDH* expression. The primer sequences can be found in Table S1.

Mitochondrial membrane potential

Cells were suspended at a density of 1×10^5/mL in culture medium containing 100 nM MitoTracker Green FM (MitoG, Thermo, M7514, Thermo Fisher Scientific) and 100 nM Image-iT TMRM Reagent (TMRM, T668, Thermo Fisher Scientific) and incubated at 37°C for 30 min. After staining, the cells were washed immediately, suspended in AutoMACS running buffer, and evaluated using an SH800. The fluorescence intensity was analyzed using FlowJo, and the numeric value was calculated by dividing the fluorescence intensity of TMRM by the fluorescence intensity of MitoG as an index of mitochondrial membrane potential.

Measurement of mitochondrial reactive oxygen species levels

Cells were suspended at a density of 1×10^5/mL in culture medium containing 5 μM MitoSOX Green mitochondrial superoxide indicator (MitoSOX, M36005, Thermo Fisher Scientific) and incubated at 37°C for 30 min. After staining, the cells were washed immediately, suspended in AutoMACS running buffer, and evaluated using an Attune flow cytometer (Thermo Fisher Scientific).

Measurements of respiratory function

An XFe96 extracellular flux analyzer (Agilent Technologies, Santa Clara, CA, USA) was used to measure cellular respiratory function. Cells were suspended in Seahorse XF D-MEM medium (Agilent Technologies) containing 10 mM glucose, 1 mM pyruvate, and 2 mM L-glutamine and seeded on XFe96-well microplates (101085-004, Agilent Technologies) at a density of 1×10^5 cells per well. After seeding, the cells were equilibrated in a non-CO_2 incubator for 20 min and used in the assay. To measure respiratory function, oligomycin (2 μM), carbonyl cyanide *p*-trifluoromethoxyphenyl hydrazone (2 μM), and rotenone/antimycin A (0.5 μM), which were adjusted using the reagents in the Seahorse XF Cell Mito Stress Test Kit (103015-100, Agilent Technologies), were sequentially added to each well after baseline measurement. The data are presented as the oxygen consumption rate (pmol/min). Basal respiration, ATP production, maximal respiration, proton leakage, spare respiratory capacity, nonmitochondrial oxygen (non-MTC), and coupling efficiency were calculated using Wave Controller 2.4 (Agilent Technologies).

Cytosolic and mitochondrial protein isolation for western blotting

Cytosolic and mitochondrial protein fractions were extracted from H9c2 cells using a Mitochondria/Cytosol Fractionation Kit (ab65320, Abcam plc., Cambridge, UK). Briefly, 1×10^6 cells were trypsinized and centrifuged at $600 \times g$ for 5 min at 4°C. Next, the cells were resuspended in cytosol extraction buffer mix, incubated on ice for 10 min, and homogenized on ice using a 29G needle. The homogenate was centrifuged at $700 \times g$ for 10 min at 4°C. The supernatant was collected and centrifuged at $10{,}000 \times g$ for 30 min at 4°C. The supernatant was used as the cytosolic fraction. The pellet was resuspended in mitochondrial extraction buffer mix, vortexed for 10 s, and used as the mitochondrial fraction.

Western blotting

Cytoplasmic protein was dissolved in RIPA buffer (182–02451, FUJIFILM Wako Pure Chemical Corporation, Richmond, VA, USA), boiled for 10 min, electrophoresed through 10% Mini-PROTEAN TGX Precast Protein Gels (4561036, Bio-Rad Laboratories), and electroblotted onto a PVDF transfer membrane (IPVH00010, Merck KGaA, Darmstadt, Germany). The membrane was blocked with PBS containing 5% skim milk and 0.05% Tween 20 (P1379, Merck KGaA) and incubated for 1 h with DRP-1 (sc-5271583, Santa Cruz Biotechnology, Dallas, TX, USA), Fis-1 (10956-1-AP, Proteintech Group, Inc., Rosemont, IL USA), GAPDH (MAB374, Merck KGaA), cytochrome *c* (sc-13156, Santa Cruz Biotechnology), cleaved caspase-3 (9664, Cell Signaling Technology), caspase 3 (9662, Cell Signaling Technology), VDAC1 (4866S, Cell Signaling Technology), and α-tubulin (66031-1-Ig, Proteintech Group) antibodies. After washing, the membrane was incubated with a 1:5,000 dilution of anti-mouse IgG (7076S, Cell Signaling Technology) or anti-rabbit IgG HRP-linked antibody (7074S, Cell Signaling Technology) in blocking buffer. Subsequently, the blots were developed using Clarity Western ECL Substrate (1705060, Bio-Rad Laboratories) or Clarity Max Western ECL Substrate (1705062, Bio-Rad Laboratories), and the protein bands were visualized using a VersaDoc or ChemiDoc Imaging System (Bio-Rad Laboratories). The protein levels were quantified using Image Lab Software Version 6.1 (4561036, Bio-Rad Laboratories).

Immunoprecipitation

Protein samples were precleared with BcMag Protein A/G Magnetic Beads (Bioclone, San Diego, CA, USA) for 2 h at room temperature, after which 6 g Fis-1 antibody (10956-1-AP, Proteintech Group) was added. Protein G beads (50 μL) were added after 2 h of incubation at room temperature. The beads were washed once with 1 mL of binding buffer (50 mM HEPES, 0.5% Triton X-100, 25 mM $MgCl_2$, 5 mM $CaCl_2$, 20 mM EDTA), once with FA500 (50 mM HEPES, 500 mM NaCl, 1 mM EDTA, 1% Triton X-100, 0.1% sodium deoxycholate), once with $LiCl_2$ buffer (10 mM Tris HCl, 250 mM $LiCl_2$, 1% Triton X-100, 0.5% sodium deoxycholate, 1 mM EDTA), and once with TES (10 mM Tris HCl, 10 mM NaCl, 1 mM EDTA). The immunoprecipitates were eluted with 75 μL RIP elution buffer (100 mM Tris HCl [pH 7.8], 10 mM EDTA, 1% SDS).

MiNA

We performed mitochondrial morphology analysis using the MiNA toolset, which was downloaded from https://github.com/stuartlab. To obtain precise results, we first improved the quality of the images. Choices for image preprocessing, including an unsharp mask and enhanced local contrast, were presented through the MiNA interface. For analysis, the image was first binarized by thresholding, assigning a maximum value of 255 to foreground pixels and a minimum value of 0 to background pixels. Next, using ImageJ's built-in skeletonization function, the binary image was converted into a skeleton that represents the features of the original image as an airframe of one-pixel-wide lines. All pixels within a skeleton were then grouped into three categories: endpoint voxels, slab voxels (area occupied by two branches), and junction voxels (area occupied by three branches). We evaluated the area of the mitochondrial footprint, slab voxels, junction voxels, mean length of branches, and the number of branches in individual cells. The mitochondrial footprint was the number of pixels in the binary image containing the signal multiplied by the area of a pixel if the calibration information was present.

Statistical analysis

The results are expressed as the means ± SDs. The statistical significance of differences among multiple groups was evaluated using Student's t test in Figure 2, and two-way ANOVA and Tukey's multiple comparisons test on Figures 3, 4, and 5 for bar graphs using GraphPad Prism. To denote the degrees of significance, stars ($^*p < 0.05$, $^{**}p < 0.01$, $^{***}p < 0.001$) were used in all figures.

DATA AND CODE AVAILABILITY

The original contributions presented in the study are included in the article/Supplemental material. Further inquiries can be directed to the corresponding author.

SUPPLEMENTAL INFORMATION

Supplemental information can be found online at https://doi.org/10.1016/j.omtm.2024.101226.

ACKNOWLEDGMENTS

The authors declare that this study was supported by funding from Remiges Ventures, Inc. (Tokyo, Japan). The funder was not involved in the study design; data collection, analysis, or interpretation; writing of this article; or decision to submit it for publication.
Our studies did not include human participants, human data, or human tissue. For the recombinant DNA experiment studies, experiments were accepted by the recombinant DNA experiment committee (2022-166) at Kyoto Prefectural University of Medicine, Japan.
We thank Ms. Sayuri Shikata for assisting with the experiments.

AUTHORS' CONTRIBUTIONS

S.G. designed the experiments, and analyzed the data; S.G. and T.T. wrote the manuscript; T.T. performed the experiments and analyzed the data with D.K., and F.T.;S.M. discussed the clinical relevance. All authors contributed to the article and approved the submitted version.

DECLARATION OF INTERESTS

S.G. is a Scientific advisor to Remiges Ventures, Inc., and has a patent related to this work.

REFERENCES

1. Cunningham, A.D., Qvit, N., and Mochly-Rosen, D. (2017). Peptides and peptidomimetics as regulators of protein-protein interactions. Curr. Opin. Struct. Biol. *44*, 59–66.
2. Lau, J.L., and Dunn, M.K. (2018). Therapeutic peptides: Historical perspectives, current development trends, and future directions. Bioorg. Med. Chem. *26*, 2700–2707.
3. Davenport, A.P., Scully, C.C.G., de Graaf, C., Brown, A.J.H., and Maguire, J.J. (2020). Advances in therapeutic peptides targeting G protein-coupled receptors. Nat. Rev. Drug Discov. *19*, 389–413.
4. Arkin, M.R., Tang, Y., and Wells, J.A. (2014). Small-molecule inhibitors of protein-protein interactions: progressing toward the reality. Chem. Biol. *21*, 1102–1114.
5. Brekke, O.H., and Sandlie, I. (2003). Therapeutic antibodies for human diseases at the dawn of the twenty-first century. Nat. Rev. Drug Discov. *2*, 52–62.
6. Boldicke, T. (2022). Therapeutic Potential of Intrabodies for Cancer Immunotherapy: Current Status and Future Directions. Antibodies *11*.
7. Lee, A.C.L., Harris, J.L., Khanna, K.K., and Hong, J.H. (2019). A Comprehensive Review on Current Advances in Peptide Drug Development and Design. Int. J. Mol. Sci. *20*, 2383.
8. Qi, X., Qvit, N., Su, Y.C., and Mochly-Rosen, D. (2013). A novel Drp1 inhibitor diminishes aberrant mitochondrial fission and neurotoxicity. J. Cell Sci. *126*, 789–802.
9. Pelay-Gimeno, M., Glas, A., Koch, O., and Grossmann, T.N. (2015). Structure-Based Design of Inhibitors of Protein-Protein Interactions: Mimicking Peptide Binding Epitopes. Angew. Chem. Int. Ed. Engl. *54*, 8896–8927.
10. Kami, D., Ishizaki, T., Taya, T., Katoh, A., Kouji, H., and Gojo, S. (2022). A novel mRNA decay inhibitor abolishes pathophysiological cellular transition. Cell Death Discov. *8*, 278.
11. Qian, Z., Dougherty, P.G., and Pei, D. (2017). Targeting intracellular protein-protein interactions with cell-permeable cyclic peptides. Curr. Opin. Chem. Biol. *38*, 80–86.
12. Siddle, K., and Hutton, J.C. (1990). Peptide Hormone Secretion: A Practical Approach (IRL Press at Oxford University Press).
13. Egel-Mitani, M., Andersen, A.S., Diers, I., Hach, M., Thim, L., Hastrup, S., and Vad, K. (2000). Yield improvement of heterologous peptides expressed in yps1-disrupted Saccharomyces cerevisiae strains. Enzyme Microb. Technol. *26*, 671–677.
14. Liao, H.X., and Spremulli, L.L. (1990). Effects of length and mRNA secondary structure on the interaction of bovine mitochondrial ribosomes with messenger RNA. J. Biol. Chem. *265*, 11761–11765.
15. Tasyurek, H.M., Altunbas, H.A., Balci, M.K., Griffith, T.S., and Sanlioglu, S. (2018). Therapeutic Potential of Lentivirus-Mediated Glucagon-Like Peptide-1 Gene Therapy for Diabetes. Hum. Gene Ther. *29*, 802–815.
16. Choi, S.H., and Lee, H.C. (2011). Long-term, antidiabetogenic effects of GLP-1 gene therapy using a double-stranded, adeno-associated viral vector. Gene Ther. *18*, 155–163.
17. Methot, D., vanKats, J.P., Lochard, N., Tremblay, F., Silversides, D.W., and Reudelhuber, T.L. (2001). Development and application of a biological peptide pump for the study of the in vivo actions of angiotensin peptides. Am. J. Hypertens. *14*, 38S–43S.
18. Jirikowski, G.F., Sanna, P.P., Maciejewski-Lenoir, D., and Bloom, F.E. (1992). Reversal of diabetes insipidus in Brattleboro rats: intrahypothalamic injection of vasopressin mRNA. Science *255*, 996–998.
19. Soltani, N., Kumar, M., Glinka, Y., Prud'homme, G.J., and Wang, Q. (2007). In vivo expression of GLP-1/IgG-Fc fusion protein enhances beta-cell mass and protects against streptozotocin-induced diabetes. Gene Ther. *14*, 981–988.
20. Zacharioudakis, E., and Gavathiotis, E. (2023). Mitochondrial dynamics proteins as emerging drug targets. Trends Pharmacol. Sci. *44*, 112–127.
21. Aung, L.H.H., Jumbo, J.C.C., Wang, Y., and Li, P. (2021). Therapeutic potential and recent advances on targeting mitochondrial dynamics in cardiac hypertrophy: A concise review. Mol. Ther. Nucleic Acids *25*, 416–443.
22. Archer, S.L. (2013). Mitochondrial dynamics–mitochondrial fission and fusion in human diseases. N. Engl. J. Med. *369*, 2236–2251.
23. Disatnik, M.H., Ferreira, J.C.B., Campos, J.C., Gomes, K.S., Dourado, P.M.M., Qi, X., and Mochly-Rosen, D. (2013). Acute inhibition of excessive mitochondrial fission after myocardial infarction prevents long-term cardiac dysfunction. J. Am. Heart Assoc. *2*, e000461.
24. Joshi, A.U., Minhas, P.S., Liddelow, S.A., Haileselassie, B., Andreasson, K.I., Dorn, G.W., 2nd, and Mochly-Rosen, D. (2019). Fragmented mitochondria released from microglia trigger A1 astrocytic response and propagate inflammatory neurodegeneration. Nat. Neurosci. *22*, 1635–1648.
25. Kodaka, M., Yang, Z., Nakagawa, K., Maruyama, J., Xu, X., Sarkar, A., Ichimura, A., Nasu, Y., Ozawa, T., Iwasa, H., et al. (2015). A new cell-based assay to evaluate myogenesis in mouse myoblast C2C12 cells. Exp. Cell Res. *336*, 171–181.
26. Manna, M.S., Tamer, Y.T., Gaszek, I., Poulides, N., Ahmed, A., Wang, X., Toprak, F.C.R., Woodard, D.R., Koh, A.Y., Williams, N.S., et al. (2021). A trimethoprim derivative impedes antibiotic resistance evolution. Nat. Commun. *12*, 2949.
27. Whitley, B.N., Engelhart, E.A., and Hoppins, S. (2019). Mitochondrial dynamics and their potential as a therapeutic target. Mitochondrion *49*, 269–283.
28. Haileselassie, B., Mukherjee, R., Joshi, A.U., Napier, B.A., Massis, L.M., Ostberg, N.P., Queliconi, B.B., Monack, D., Bernstein, D., and Mochly-Rosen, D. (2019). Drp1/Fis1 interaction mediates mitochondrial dysfunction in septic cardiomyopathy. J. Mol. Cell. Cardiol. *130*, 160–169.
29. Tadokoro, T., Ikeda, M., Ide, T., Deguchi, H., Ikeda, S., Okabe, K., Ishikita, A., Matsushima, S., Koumura, T., Yamada, K.-I., et al. (2020). Mitochondria-dependent ferroptosis plays a pivotal role in doxorubicin cardiotoxicity. JCI Insight *5*, e132747.
30. Valente, A.J., Maddalena, L.A., Robb, E.L., Moradi, F., and Stuart, J.A. (2017). A simple ImageJ macro tool for analyzing mitochondrial network morphology in mammalian cell culture. Acta Histochem. *119*, 315–326.
31. Fosgerau, K., and Hoffmann, T. (2015). Peptide therapeutics: current status and future directions. Drug Discov. Today *20*, 122–128.
32. Reese, H.R., Shanahan, C.C., Proulx, C., and Menegatti, S. (2020). Peptide science: A "rule model" for new generations of peptidomimetics. Acta Biomater. *102*, 35–74.
33. Banaszynski, L.A., and Wandless, T.J. (2006). Conditional control of protein function. Chem. Biol. *13*, 11–21.
34. Ramadurgum, P., Woodard, D.R., Daniel, S., Peng, H., Mallipeddi, P.L., Niederstrasser, H., Mihelakis, M., Chau, V.Q., Douglas, P.M., Posner, B.A., and Hulleman, J.D. (2020). Simultaneous Control of Endogenous and User-Defined Genetic Pathways Using Unique ecDHFR Pharmacological Chaperones. Cell Chem. Biol. *27*, 622–634.e6.
35. Wang, X., and Marchisio, M.A. (2021). Synthetic polycistronic sequences in eukaryotes. Synth. Syst. Biotechnol. *6*, 254–261.
36. Subbiah, M., Khattar, S.K., Collins, P.L., and Samal, S.K. (2011). Mutations in the fusion protein cleavage site of avian paramyxovirus serotype 2 increase cleavability and syncytium formation but do not increase viral virulence in chickens. J. Virol. *85*, 5394–5405.
37. Liu, Z., Chen, O., Wall, J.B.J., Zheng, M., Zhou, Y., Wang, L., Vaseghi, H.R., Qian, L., and Liu, J. (2017). Systematic comparison of 2A peptides for cloning multi-genes in a polycistronic vector. Sci. Rep. *7*, 2193.
38. Huang, E.Y.-C., Frederick, J., McKinney, K., Henderson, C., Cheung-Ong, K., Bolen, J., Kelsey, S.M., Morin, M., Gurumurthy, S., Benenato, K., et al. (2017). Messenger ribonucleic acids for the production of intracellular binding polypeptides and methods of use thereof US2021/0206818A1.
39. Rezaei Araghi, R., and Keating, A.E. (2016). Designing helical peptide inhibitors of protein-protein interactions. Curr. Opin. Struct. Biol. *39*, 27–38.
40. Laxio Arenas, J., Kaffy, J., and Ongeri, S. (2019). Peptides and peptidomimetics as inhibitors of protein-protein interactions involving beta-sheet secondary structures. Curr. Opin. Chem. Biol. *52*, 157–167.
41. Dyson, H.J., and Wright, P.E. (2005). Intrinsically unstructured proteins and their functions. Nat. Rev. Mol. Cell Biol. *6*, 197–208.

42. Shimizu, T., Takahashi, N., Huber, V.J., Asawa, Y., Ueda, H., Yoshimori, A., Muramatsu, Y., Seimiya, H., Kouji, H., Nakamura, H., and Oguri, H. (2021). Design and synthesis of 14 and 15-membered macrocyclic scaffolds exhibiting inhibitory activities of hypoxia-inducible factor 1alpha. Bioorg. Med. Chem. *30*, 115949.

43. Glas, A., Bier, D., Hahne, G., Rademacher, C., Ottmann, C., and Grossmann, T.N. (2014). Constrained peptides with target-adapted cross-links as inhibitors of a pathogenic protein-protein interaction. Angew. Chem. Int. Ed. Engl. *53*, 2489–2493.

44. Reguera, L., and Rivera, D.G. (2019). Multicomponent Reaction Toolbox for Peptide Macrocyclization and Stapling. Chem. Rev. *119*, 9836–9860.

45. Carvajal, L.A., Neriah, D.B., Senecal, A., Benard, L., Thiruthuvanathan, V., Yatsenko, T., Narayanagari, S.R., Wheat, J.C., Todorova, T.I., Mitchell, K., et al. (2018). Dual inhibition of MDMX and MDM2 as a therapeutic strategy in leukemia. Sci. Transl. Med. *10*, eaao3003.

46. Saleh, M.N., Patel, M.R., Bauer, T.M., Goel, S., Falchook, G.S., Shapiro, G.I., Chung, K.Y., Infante, J.R., Conry, R.M., Rabinowits, G., et al. (2021). Phase 1 Trial of ALRN-6924, a Dual Inhibitor of MDMX and MDM2, in Patients with Solid Tumors and Lymphomas Bearing Wild-type TP53. Clin. Cancer Res. *27*, 5236–5247.

47. Al Shaer, D., Al Musaimi, O., Albericio, F., and de la Torre, B.G. (2020). 2019 FDA TIDES (Peptides and Oligonucleotides) Harvest. Pharmaceuticals *13*, 40.

48. Szabó, G.T., Mahiny, A.J., and Vlatkovic, I. (2022). COVID-19 mRNA vaccines: Platforms and current developments. Mol. Ther. *30*, 1850–1868.

49. Baden, L.R., El Sahly, H.M., Essink, B., Kotloff, K., Frey, S., Novak, R., Diemert, D., Spector, S.A., Rouphael, N., Creech, C.B., et al. (2021). Efficacy and Safety of the mRNA-1273 SARS-CoV-2 Vaccine. N. Engl. J. Med. *384*, 403–416.

50. Polack, F.P., Thomas, S.J., Kitchin, N., Absalon, J., Gurtman, A., Lockhart, S., Perez, J.L., Pérez Marc, G., Moreira, E.D., Zerbini, C., et al. (2020). Safety and Efficacy of the BNT162b2 mRNA Covid-19 Vaccine. N. Engl. J. Med. *383*, 2603–2615.

51. Hou, X., Zaks, T., Langer, R., and Dong, Y. (2021). Lipid nanoparticles for mRNA delivery. Nat. Rev. Mater. *6*, 1078–1094.

52. Paunovska, K., Loughrey, D., and Dahlman, J.E. (2022). Drug delivery systems for RNA therapeutics. Nat. Rev. Genet. *23*, 265–280.

53. Biscans, A., Coles, A., Haraszti, R., Echeverria, D., Hassler, M., Osborn, M., and Khvorova, A. (2019). Diverse lipid conjugates for functional extra-hepatic siRNA delivery in vivo. Nucleic Acids Res. *47*, 1082–1096.

54. Lee, B., Lee, K., Panda, S., Gonzales-Rojas, R., Chong, A., Bugay, V., Park, H.M., Brenner, R., Murthy, N., and Lee, H.Y. (2018). Nanoparticle delivery of CRISPR into the brain rescues a mouse model of fragile X syndrome from exaggerated repetitive behaviours. Nat. Biomed. Eng. *2*, 497–507.

55. Breda, L., Papp, T.E., Triebwasser, M.P., Yadegari, A., Fedorky, M.T., Tanaka, N., Abdulmalik, O., Pavani, G., Wang, Y., Grupp, S.A., et al. (2023). In vivo hematopoietic stem cell modification by mRNA delivery. Science *381*, 436–443.

56. Vavassori, V., Ferrari, S., Beretta, S., Asperti, C., Albano, L., Annoni, A., Gaddoni, C., Varesi, A., Soldi, M., Cuomo, A., et al. (2023). Lipid nanoparticles allow efficient and harmless ex vivo gene editing of human hematopoietic cells. Blood *142*, 812–826.

57. Tarakanchikova, Y., Muslimov, A., Sergeev, I., Lepik, K., Yolshin, N., Goncharenko, A., Vasilyev, K., Eliseev, I., Bukatin, A., Sergeev, V., et al. (2020). A highly efficient and safe gene delivery platform based on polyelectrolyte core-shell nanoparticles for hard-to-transfect clinically relevant cell types. J. Mater. Chem. B *8*, 9576–9588.

58. Chen, W., Zhao, H., and Li, Y. (2023). Mitochondrial dynamics in health and disease: mechanisms and potential targets. Signal Transduct. Target. Ther. *8*, 333.

59. Galloway, C.A., Lee, H., Brookes, P.S., and Yoon, Y. (2014). Decreasing mitochondrial fission alleviates hepatic steatosis in a murine model of nonalcoholic fatty liver disease. Am. J. Physiol. Gastrointest. Liver Physiol. *307*, G632–G641.

60. Aoyagi, Y., Hayashi, Y., Harada, Y., Choi, K., Matsunuma, N., Sadato, D., Maemoto, Y., Ito, A., Yanagi, S., Starczynowski, D.T., and Harada, H. (2022). Mitochondrial Fragmentation Triggers Ineffective Hematopoiesis in Myelodysplastic Syndromes. Cancer Discov. *12*, 250–269.